

Analytical Approach to Predicting Temperature Fields in Multi-Layered Pavement Systems

Dong Wang¹, Jeffery R. Roesler, P.E., Member ASCE² and Da-Zhi Guo³

Abstract: An accurate and rapid estimation of the pavement temperature field is desired to better predict pavement responses and for pavement system design. In this paper, an innovative method to derive the theoretical solution of an axisymmetric temperature field in a multi-layered pavement system is presented. The multi-layered pavement system was modeled as a two-dimensional heat transfer problem. The temperature at any location (r, z) and any time t in an N-layer pavement system can be calculated by using the derived analytical solution. Hankel integral transform with respect to the radial coordinate is utilized in the derivation of the solution. The interpolatory trigonometric polynomials based on discrete Fourier transform are used to fit the measured air temperatures and solar radiation intensities during a day, which are essential components in the boundary condition for the underlying heat transfer problem. A FORTRAN program was coded to implement this analytical solution. Measured field temperature results from a rigid pavement system demonstrate that the derived analytical solution generates reasonable temperature profiles in the concrete slab.

CE Database subject headings: Temperature distribution; Layered systems; Flexible pavements; Rigid pavements; Heat transfer; Temperature effects.

¹ Graduate Research Assistant (Corresponding author), Dept. of Civil and Environmental Engineering, University of Illinois at Urbana-Champaign. B231 Newmark Civil Engineering Laboratory, MC-250, 205 North Mathews Avenue, Urbana, IL 61801. Tel: (217) 244-1803. E-mail: dongwang@uiuc.edu

² Associate Professor, Dept. of Civil and Environmental Engineering, University of Illinois at Urbana-Champaign. 1211 Newmark Civil Engineering Laboratory, MC-250, 205 North Mathews Avenue, Urbana, IL 61801. Tel: (217) 265-0218. E-mail: jroesler@uiuc.edu

³ Emeritus Professor, School of Transportation Science and Engineering, Harbin Institute of Technology. No. 202, Haihe Avenue, Nangang District, Harbin, China, 150090. Tel: (86) 451-8628 2116

INTRODUCTION

It is well known that temperature variation in pavement layers play an important role in the performance of both flexible and rigid pavement systems (1). In flexible pavement systems, the surface layer is usually made of hot-mix asphalt (HMA), which is a visco-elastic material and its behavior is highly related to its temperature, i.e., HMA responds like an elastic solid under low temperature and strain conditions; on the other hand, it also acts as a viscous material at high temperature in the sense that the deformation due to traffic loading cannot fully recovered within a finite time period under the unloading condition (2). Therefore, an accurate prediction of the temperature profile in the HMA layer is desired when selecting the asphalt binder and predicting performance. For rigid pavement design, the thermal curling stress in the concrete slab cannot be ignored (3) and by some manner must be added to the traffic loading stresses (4,5). In order to accurately capture the critical thermal stresses in the PCC slab, the temperature profile throughout the day must be known.

Many research efforts have been taken on developing different mathematical models to predict temperature profile within a pavement system. Most of published results on this topic can be fitted into statistics-based models or heat transfer models.

Statistics-Based Pavement Temperature Prediction Models

The statistics-based regression formulae are usually developed based on large databases of climatic, meteorological and geographical factors, such as air temperature, wind speed, solar radiation and latitude etc, as well as the measured field pavement temperatures. Rumney and Jimenez (7) approximated temperature at the surface and at a 2-inch depth based on air temperature and hourly solar radiation. Lukanen et al. (8) predicted the seven-day average high pavement temperature using seven-day average high air temperature. More recently, Diefenderfer et al. (9) calculated the maximum and minimum temperature at any depth by using air temperature, daily solar radiation and depth within the pavement. Empirical formulae are usually applied to rapidly predict certain extreme temperatures within a pavement system or a specific temperature at a given pavement depth. However, the disadvantage of these types of formulae is that they give reasonable prediction for the input data included within the original sample database, but do not guarantee the accuracy of prediction for the input data outside the original sample database.

Heat Transfer Models

The existing heat transfer models that predict pavement temperature profile are usually solved using a numerical method, which typically consist of four steps. Firstly, the governing equation to account for the heat conduction within a pavement must be set up, which is usually a one-dimensional (1-D) or two-dimensional (2-D) heat transfer model represented by a time-dependent partial differential equation (PDE). Secondly, an appropriate boundary condition must be established linking the climatic parameters with the pavement surface temperature. This link is accomplished by analyzing the energy balance at the pavement surface. Thirdly, the spatial domain needs to be discretized using a numerical method, such as finite-difference method,

finite-element method, etc., which results in a large system of ordinary differential equations (ODEs) in time. Fourthly, an appropriate time-integrator is required to solve these ODEs. For example, this time-integrator can be either a linear multi-step method or a Runge-Kutta method.

Dempsey and Thompson (10) were one of the first researchers to develop a numerical simulation approach by using 1-D heat transfer model and an explicit finite-difference method. Hsieh et al. (11) proposed a three-dimensional numerical model to calculate the temperature distribution within concrete pavement. Recently, Rasmussen et al. (12) and Schindler et al. (13) proposed models to predict the temperature distribution in the early-age PCC pavement by incorporating both the climatic factors and the heat of hydration of cementitious materials into the models using a finite element or a 1-D finite-difference method, respectively. Yavuzturk et al. (14) simulated temperature fluctuations in asphalt pavements due to thermal environmental conditions by using a 2-D finite-difference method.

Analytical Approaches

As far as analytical solution of temperature profiles through a multi-layer pavement system is concerned, very few results are available due to the complexity encountered in deriving the closed-form analytical solution. Barber (6) calculated the maximum pavement temperature from weather reports for a 1-layer system. Solaimanian and Kennedy (15) proposed a simple analytical equation to predict the maximum pavement surface temperature based on maximum air temperature and hourly solar radiation. Liang and Niu (16) derived a closed-form analytical solution of temperature distribution in a 3-layer system using a simplified boundary condition, which only involved the convection of heat between the atmosphere and pavement surface but not any solar radiation effect.

The main hurdle associated with the numerical methods for predicting pavement temperature field is that the initial pavement temperature distribution (called initial condition) must be available in order to calculate temperature field for the later time, since a time-dependent PDE problem essentially needs to be solved. However, the initial pavement temperature profile is typically not available. To remove this hurdle, a 2-D axisymmetric approach for analytically predicting the temperature field in an N-layered pavement system is proposed in this paper when the initial pavement temperature profile is not known, which extends the analytical solution for a 3-layer pavement system by Liang and Niu (16). Moreover, the proposed model handles measured solar radiation and considers irradiation. The proposed temperature solution is valid for pavement systems with N-layers, at any depth of pavement, z , radial direction, r and time, t during the day using measured climatic data and pavement material properties. This model can predict temperature profiles in both multi-layered flexible and rigid pavement systems assuming the thermal properties of the materials are known.

MATHEMATICAL TEMPERATURE MODEL

The temperature distribution in a multi-layered pavement system, shown in Fig. 1, can be modeled as a heat transfer problem, where h_i = layer thickness (m), λ_i = thermal conductivity (Kcal/m-hr-°C), α_i = thermal diffusivity (m²/hr), and $T_i(r, z, t)$ = temperature (°C) for layer i . The

thickness of the last layer (subgrade), h_n , is assumed to be infinite along the positive z direction. All materials in the multi-layered systems are assumed to be continuous, homogeneous, and isotropic. The temperature profile in the layer i , $T_i(r, z, t)$ is assumed to be axisymmetric. One advantage of this assumption is that the thermal stresses due to temperature change can be easily incorporated with the traffic loading stresses by using the layered elastic theory, since the latter is also considered to be axisymmetric (17).

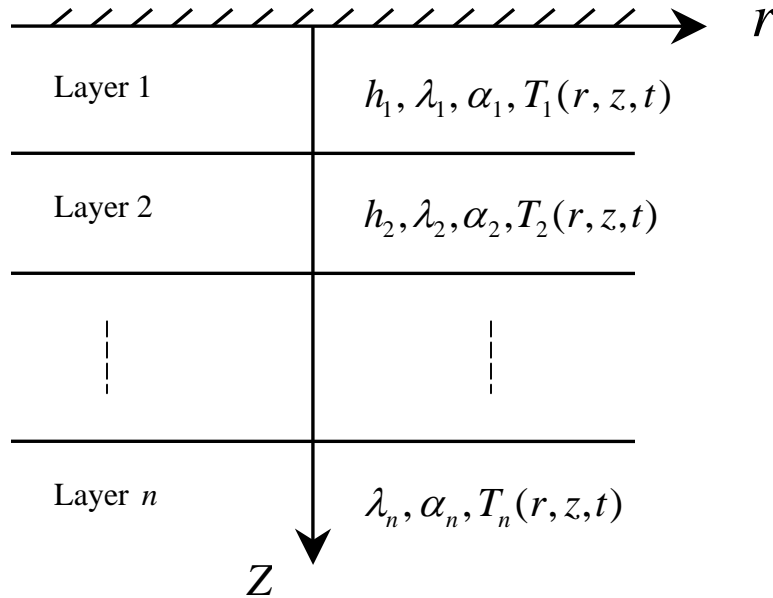


Figure1: Multi-layered Pavement System

In cylindrical coordinate system, the 2-D axisymmetric heat transfer problem can be modeled with the following governing time-dependent PDE:

$$\frac{\partial T_i}{\partial t} = \alpha_i \nabla^2 T_i \quad \text{for } H_{i-1} \leq z \leq H_i \quad (1)$$

where $H_i = \sum_{k=1}^i h_k$; $\nabla^2 = \frac{\partial^2}{\partial r^2} + \frac{1}{r} \frac{\partial}{\partial r} + \frac{\partial^2}{\partial z^2}$, Laplace operator in cylindrical coordinate for the axisymmetric problem.

It is assumed that the temperature and heat flow are continuous along the interface of two consecutive layers, i.e.

$$T_i(r, H_i, t) = T_{i+1}(r, H_i, t) \quad (2a)$$

$$\lambda_i \frac{\partial T_i}{\partial z}(r, H_i, t) = \lambda_{i+1} \frac{\partial T_{i+1}}{\partial z}(r, H_i, t) \quad (2b)$$

The bounded temperature at an infinite depth is given by

$$|T_n(r, z, t)| \leq M \quad \text{as } z \rightarrow \infty \quad (3)$$

where M is a constant.

The boundary conditions (BCs) play an important role in computing the temperature profile in multi-layered pavement systems. The temperature at the pavement surface is greatly influenced by meteorological and geographical factors, such as air temperature, solar radiation, wind speed, latitude and elevation of the pavement (10, 15, 18). The BCs can be set up by analyzing the energy balance at the pavement surface. Mathematically, it is expressed as (19)

$$q = P + R \quad (4)$$

where q = heat flux into pavement (Kcal/m²-hr); P = heat flux caused by the convection due to temperature difference between atmosphere and pavement surface (Kcal/m²-hr); R = net solar radiation flux (Kcal/m²-hr).

By Fourier's law of conduction, heat flow into pavement, q , is pointed to the direction of temperature gradient $-\nabla T_1$ and calculated as follows

$$q = -\lambda_1 \frac{\partial T_1}{\partial z}(r, 0, t) \quad (5)$$

The convection energy, P , is calculated as

$$P = B(T_a(t) - T_1(r, 0, t)) \quad (6)$$

Where $T_a(t)$ = air temperature (°C); $T_1(r, 0, t)$ = pavement surface temperature (°C); B = pavement surface convection coefficient (Kcal/m²-hr-°C), which primarily depends on the surface roughness, wind speed, air temperature and pavement surface temperature. Branco et al. (20) approximated it as:

$$B = 0.8598(6 + 3.7v)$$

Where v = wind speed (m/s); and 0.8598 is the unit conversion constant when the unit is converted from W/m²-°C to Kcal/m²-hr-°C.

The net radiation energy, R , is given by

$$R = a_s Q(t) - F(t) \quad (7)$$

Where a_s = surface absorptivity to the total solar radiation (dimensionless); $Q(t)$ = solar radiation flux ($\text{Kcal/m}^2 \cdot \text{hr}$); $F(t)$ = irradiation flux emitted by pavement surface ($\text{Kcal/m}^2 \cdot \text{hr}$).

Substituting equations (5)-(7) into equation (4) yields the following BC

$$-\lambda_1 \frac{\partial T_1}{\partial z}(r, 0, t) = a_s Q(t) - F(t) + B(T_a(t) - T_1(r, 0, t)) \quad (8)$$

Eqs. (1)-(3) and (8) constitute the mathematical modeling of temperature field in multi-layered pavement systems. In order to analytically derive the solution of temperature field, continuous functions for representing $Q(t)$, $F(t)$ and $T_a(t)$ are desired. In this paper, $Q(t)$ and $T_a(t)$ are assumed to be measured at a half-hour interval during a day. Interpolatory trigonometric polynomials, based on discrete Fourier transform, can then be used to fit the daily measured data of $Q(t)$ and $T_a(t)$ as described below (21).

Solar Radiation, $Q(t)$

$$Q(t) = \frac{a_0}{2} + \frac{a_m}{2} \cos\left(\frac{m\pi}{12}(t-12)\right) + \sum_{k=1}^{m-1} \left(a_k \cos\left(\frac{k\pi}{12}(t-12)\right) + b_k \sin\left(\frac{k\pi}{12}(t-12)\right) \right) \quad (9)$$

with

$$a_k = \frac{1}{m} \sum_{j=0}^{2m-1} q_j \cos\left(\frac{k\pi}{m}(j-m)\right) \quad \text{for each } k = 0, 1, \dots, m \quad (10a)$$

$$b_k = \frac{1}{m} \sum_{j=0}^{2m-1} q_j \sin\left(\frac{k\pi}{m}(j-m)\right) \quad \text{for each } k = 1, 2, \dots, m-1 \quad (10b)$$

where $m = 24$ if 48 equally spaced sample points are used; $t = 0$ at 0:00 a.m. and q_j is the measured solar radiation intensity value at time $t_j = 0.5 * j$ for $j = 0, 1, \dots, 2m-1$.

Ambient Temperature, $T_a(t)$

The approximation of ambient temperature, $T_a(t)$ can be analogously treated by

$$T_a(t) = \frac{c_0}{2} + \frac{c_m}{2} \cos\left(\frac{m\pi}{12}(t-12)\right) + \sum_{k=1}^{m-1} \left(c_k \cos\left(\frac{k\pi}{12}(t-12)\right) + d_k \sin\left(\frac{k\pi}{12}(t-12)\right) \right) \quad (11)$$

With

$$c_k = \frac{1}{m} \sum_{j=0}^{2m-1} T_j \cos\left(\frac{k\pi}{m}(j-m)\right) \quad \text{for each } k = 0, 1, \dots, m \quad (12a)$$

$$d_k = \frac{1}{m} \sum_{j=0}^{2m-1} T_j \sin\left(\frac{k\pi}{m}(j-m)\right) \quad \text{for each } k = 1, 2, \dots, m-1 \quad (12b)$$

Where $m=24$ and T_j is the measured air temperature at time t_j as defined above.

Irradiation Energy emitted by pavement surface $F(t)$

A fourth order equation to account for the irradiation emitted by pavement surface was used in reference (10), which was given by

$$F(t) = (1 - N\bar{W})\sigma[\varepsilon T_1^4(r,0,t) - T_{air}^4(G - J(10^{-\rho p}))] \quad (13)$$

where N = cloud-base factor; \bar{W} = percentage of cloud cover at night; σ = Stefan-Boltzmann constant; ε = emissivity of radiation by pavement surface; $T_1(r,0,t)$ = Rankine temperature of pavement surface; T_{air} = Rankine air temperature; G, J, ρ and p are model parameters. Barber (6) took irradiation into consideration by discounting the daily solar radiation intensity. For simplicity, the nonlinearity in the BC imposed by $F(t)$ is avoided in this paper by modifying the convection coefficient, B and pavement surface absorptivity a_s (19).

Temperature Variation Along the Radial Direction

Finally, to account for the temperature variation along the radial direction, a non-dimensional calibration term $f(r)$ is introduced in the BC as follows

$$f(r) = e^{-\mu r} \quad (14)$$

where μ can be fitted by using the measured pavement temperature in the radial direction. In this paper, $\mu = 0.001$ to 0.002 (1/m) is assumed when the temperature difference between the center of pavement cross section and shoulder is 5 to 10 °C, respectively (19). Also the unit of r is in meters in eq. (14). Thus, the BCs may be modified as

$$-\lambda_1 \frac{\partial T_1}{\partial z}(r,0,t) = B \left[f(r) \left(T_a(t) + \frac{a_s Q(t) - F(t)}{B} \right) - T_1(r,0,t) \right] \quad (15)$$

Substituting eqs. (9), (11), and (14) into eq. (15) and taking $F(t)$ into consideration by modifying B and a_s yield the following BCs

$$\begin{aligned}
-\lambda_1 \frac{\partial T_1}{\partial z}(r,0,t) = & B\{e^{-\mu r} [\frac{c_0}{2} + \frac{a_s a_0}{2B} + (\frac{c_m}{2} + \frac{a_s a_m}{2B}) \sin(m\bar{t} + \frac{\pi}{2}) \\
& + \sum_{k=1}^{m-1} [(c_k + \frac{a_s}{B} a_k) \sin(k\bar{t} + \frac{\pi}{2}) + (d_k + \frac{a_s}{B} b_k) \sin(k\bar{t})]] - T_1(r,0,t)\}
\end{aligned} \tag{16}$$

where $\bar{t} = \frac{\pi}{12}(t - 12)$.

THEORETICAL SOLUTION OF PAVEMENT TEMPERATURE PROFILE

The sinusoidal terms in the right hand side of eq. (16) only differ in magnitudes, frequencies, and phase angles. In order to facilitate presentation of the analytical solution of $T_i(r, z, t)$, the following sample BC is introduced from which the solution of $T_i(r, z, t)$ will be developed:

$$-\lambda_1 \frac{\partial T_1}{\partial z}(r,0,t) = B\{e^{-\mu r} \cdot A \sin(\omega t) - T_1(r,0,t)\} \tag{17}$$

where $A = \text{constant}$ ($^{\circ}\text{C}$), representing the magnitude of each sine function in eq. (16).

It is clear that the final solution of $T_i(r, z, t)$ based on the linear BC in eq. (16) can be obtained by using the principle of superposition, i.e., it equals the summation of temperature values based on each sinusoidal term in eq. (16) plus the constant terms, i.e. $\frac{a_0}{2}$ and $\frac{a_s c_0}{2B}$ in eq. (16). Furthermore, it is observed that $\sin(\omega t)$ on the right hand side of eq. (17) can be related to the complex value $e^{j\omega t}$ by using the Euler formula:

$$e^{j\omega t} = \cos(\omega t) + j \sin(\omega t) \tag{18}$$

where j is the imaginary unit number with $j^2 = -1$.

Since relating $\sin(\omega t)$ with $e^{j\omega t}$ can greatly facilitate the derivation of the analytical solution, the temperature distribution is first derived in the complex plane, $Y_i(r, z, t)$, then the desired solution of temperature profile for the 2-D heat transfer problem, $T_i(r, z, t)$ is simply the imaginary part of $Y_i(r, z, t)$. To easily present the derivation, the governing equation and the constraint conditions for this 2-D heat transfer problem are represented in terms of the complex variables, $Y_i(r, z, t)$ as follows:

Two-Dimensional Heat Transfer Equation

$$\frac{\partial Y_i}{\partial t} = \alpha_i \nabla^2 Y_i \quad \text{for } H_{i-1} \leq z \leq H_i \tag{19}$$

where $H_i = \sum_{k=1}^i h_k$

Interlayer Contact Condition

$$Y_i(r, H_i, t) = Y_{i+1}(r, H_i, t) \quad (20a)$$

$$\lambda_i \frac{\partial Y_i}{\partial z}(r, H_i, t) = \lambda_{i+1} \frac{\partial Y_{i+1}}{\partial z}(r, H_i, t) \quad (20b)$$

Bounded Temperature Value at Infinite Depth

$$|Y_n(r, z, t)| \leq M \quad \text{as } z \rightarrow \infty \quad (21)$$

where $M = \text{constant}$.

Boundary Condition

$$-\lambda_1 \frac{\partial Y_1}{\partial z}(r, 0, t) = B\{e^{-\mu r} \cdot Ae^{j\omega t} - Y_1(r, 0, t)\} \quad (22)$$

The following outlines the main steps involved in deriving the analytical solution of $Y_i(r, z, t)$:

(1) By using the approach of separation of variables (22), $Y_i(r, z, t)$ can be expressed as

$$Y_i(r, z, t) = u_i(r, z) \cdot e^{j\omega t} \quad (23)$$

It follows that

$$\frac{\partial Y_i}{\partial t} = j\omega Y_i \quad (24)$$

(2) Substituting of eqs. (23), (24) into eqn. (19) yields

$$j\omega \cdot u_i(r, z) = \alpha_i \cdot \nabla^2 u_i(r, z) \quad (25)$$

(3) Hankel integral transform is employed to solve eq. (25). Let $\bar{\phi}(\xi)$ be the Hankel transform of order zero of an arbitrary function $\phi(r)$ and then from reference (23)

$$\bar{\phi}(\xi) = \int_0^{\infty} r\phi(r)J_0(\xi r)dr \quad (26)$$

Where $J_0(\xi r)$ = the first kind of Bessel function of order zero.

The inverse Hankel transform of order zero of $\bar{\phi}(\xi)$ is

$$\phi(r) = \int_0^{\infty} \xi \bar{\phi}(\xi) J_0(\xi r) d\xi \quad (27)$$

Also, the Hankel transform of order zero of $\frac{d^2\phi}{dr^2}(r) + \frac{1}{r} \frac{d\phi}{dr}(r)$ is given by formula (5-4-7) in reference (23)

$$\int_0^{\infty} r \left(\frac{d^2}{dr^2} + \frac{1}{r} \frac{d}{dr} \right) \phi(r) J_0(\xi r) dr = -\xi^2 \bar{\phi}(\xi) \quad (28)$$

(4) Applying Hankel transform of order zero to the both sides of eq. (25) with respect to r in conjunction with eq. (28) yields

$$\frac{\partial^2 \bar{u}_i}{\partial z^2}(\xi, z) - \left(\xi^2 + \frac{\omega}{\alpha_i} j \right) \bar{u}_i(\xi, z) = 0 \quad (29)$$

(5) Solving eq. (29) in the Hankel domain gives

$$\bar{u}_i(\xi, z) = C_i e^{-\xi \cdot z \sqrt{1 + j \frac{\omega}{\alpha_i \xi^2}}} + D_i e^{\xi \cdot z \sqrt{1 + j \frac{\omega}{\alpha_i \xi^2}}} \quad (30)$$

where C_i, D_i are constants for layer i , which are determined by using the constraint conditions.

(6) Taking inverse Hankel transform of order zero of eq. (30) and considering eq. (23) yield the temperature of layer i in the complex plane, $Y_i(r, z, t)$ as follows:

$$Y_i(r, z, t) = \int_0^{\infty} \xi [C_i e^{-\xi \cdot z \cdot M_i} \cdot e^{-j \xi \cdot z \cdot N_i} + D_i e^{\xi \cdot z \cdot M_i} \cdot e^{j \xi \cdot z \cdot N_i}] \cdot J_0(\xi r) e^{j \omega t} d\xi \quad (31)$$

Where M_i and N_i are defined in the Appendix.

(7) Determining coefficients of C_i and D_i :

(a) The relationship between C_{i+1}, D_{i+1} and C_i, D_i can be exploited in the following matrix-vector form by using eq. (31) and the interlayer contact conditions stated in eq. (20):

$$\begin{bmatrix} C_{i+1} \\ D_{i+1} \end{bmatrix} = \begin{bmatrix} e^{-\xi \cdot H_i(M_i - M_{i+1})} \cdot P_i^{11} & e^{\xi \cdot H_i(M_i + M_{i+1})} \cdot P_i^{12} \\ e^{-\xi \cdot H_i(M_i + M_{i+1})} \cdot P_i^{21} & e^{\xi \cdot H_i(M_i - M_{i+1})} \cdot P_i^{22} \end{bmatrix} \cdot \begin{bmatrix} C_i \\ D_i \end{bmatrix} \quad (32)$$

Where $P_i^{11}, P_i^{12}, P_i^{21}, P_i^{22}$ are defined in the Appendix.

(b) The recursive formula linking C_i, D_i and C_1, D_1 can be further deduced from eq. (32) as follows:

$$\begin{bmatrix} C_i \\ D_i \end{bmatrix} = \begin{bmatrix} e^{\xi \cdot H_{i-1}(M_i + M_{i-1})} & 0 \\ 0 & e^{-\xi \cdot H_{i-1}(M_i - M_{i-1})} \end{bmatrix} \cdot \begin{bmatrix} e^{-2\xi \cdot H_1 M_1} \cdot R_{i-1}^{11} & R_{i-1}^{12} \\ e^{-2\xi \cdot H_1 M_1} \cdot R_{i-1}^{21} & R_{i-1}^{22} \end{bmatrix} \cdot \begin{bmatrix} C_1 \\ D_1 \end{bmatrix} \quad (33)$$

where $i = 2, 3, \dots, n$; R_i^{kl} ($k, l = 1, 2$) are defined in the Appendix, and eq. (33) can be easily proved by using the method of mathematical induction.

(c) Bounded solution for $Y_n(r, z, t)$ as $z \rightarrow \infty$ indicates that $D_n = 0$ from eq. (31), and the relationship between C_1 and D_1 can be further derived by setting $D_n = 0$ in eq. (33) as follows:

$$D_1 = -e^{-2\xi \cdot H_1 M_1} \frac{R_{n-1}^{21}}{R_{n-1}^{22}} C_1 \quad (34)$$

(d) C_1 and D_1 can be obtained by using eq. (34) in conjunction with the B.C. in eq. (22).

Furthermore, C_i and D_i for the i th layer can be solved by using eq. (33).

(e) Once C_i and D_i are determined, the desired solution $T_i(r, z, t)$ for the i th layer is simply the imaginary part of $Y_i(r, z, t)$ in eq. (31). The expression for $T_i(r, z, t)$ is given in eq. (35) with all the symbols defined in the Appendix.

$$T_i(r, z, t) = \int_0^\infty \xi [\Delta_{i1} e^{\xi [H_{i-1}(M_i + M_{i-1}) - z \cdot M_i]} \cdot \sin(\omega t + \delta_{i1} - \xi z N_i) + \Delta_{i2} e^{\xi [-H_{i-1}(M_i - M_{i-1}) + z \cdot M_i]} \cdot \sin(\omega t + \delta_{i2} + \xi z N_i)] J_0(\xi r) d\xi \quad (35)$$

Numerical Implementation of Analytical Solution

As shown in eqn. (35), an integral with respect to ξ ranging from 0 to ∞ must be solved in order to calculate the temperature distribution $T_i(r, z, t)$ for the i th layer, and this can be solved numerically. A computer cannot handle an ∞ upper limit of integration, thus, an appropriate truncated upper limit, x_u , has to be chosen, which can be determined by a convergence test of $T_i(r, z, t)$. One such convergence test example is shown in Table 2 in the next section. In this

paper, the composite 16-point Gaussian Quadrature formula (21) is employed to resolve the integral in eq. (35), i.e., interval $[0, x_u]$ is firstly divided into some smaller subintervals, then the 16-point Gaussian Quadrature formula is applied in each subinterval to obtain the solution for $T_i(r, z, t)$.

MODEL VERIFICATION WITH FIELD DATA

A FORTRAN computer program was developed to predict the temperature profile in a multi-layered pavement system by using the above analytical solution of the temperature field. For the model validation, the computed temperature profile in a continuously reinforced concrete pavement (CRCP) test section is compared with measured field data from the Advanced Transportation Research and Engineering Laboratory (ATREL) in Illinois, USA (24). The CRCP test sections consist of concrete slab (0.254m) with continuous reinforcing steel, asphalt concrete base (0.102m) and aggregate subbase (0.152m) all supported on a silty-clay soil layer. Temperatures at five different slab depth locations, i.e., 0.0254m, 0.0762m, 0.127m, 0.1778m and 0.2286m from pavement surface, along with several climatic parameters, such as wind speed, wind direction and solar radiation were measured at a half-hour interval.

In this paper, temperatures in CRCP test section at the aforementioned five slab depth locations were continuously predicted using the above analytical solution for 71.5 hours at a half-hour interval in both winter and summer conditions, i.e. starting from 0:00 a.m. on January 12, 2003 until 11:30 p.m. on January 14, 2003 and from 0:00 a.m. on June 28, 2003 until 11:30 p.m. on June 30, 2003. Half-hour measured air temperature and solar radiation for each three-day period were employed to generate the fitting interpolatory trigonometric polynomials as shown in Figures 2. The other input parameters including the typical thermal properties for these pavement materials (5,10) are listed in Table 1. To determine the appropriate upper limit, x_u , of the integral in eq. (35), numerical convergence tests for the inverse Hankel integral transform is carried out using the above input parameters. The numerical implementation indicated that the improper integral in eq. (35) usually converged faster as value of z increased, thus the dimensionless quantity x_u is selected as

$$x_u = \text{int}\left(\frac{H_{n-1}}{3z}\right) \cdot 3I \quad (36)$$

where int = an integer function converting its argument into an largest integer less than or equal to itself; I = test number; H_{n-1} = sum of thickness of pavement layers except subgrade layer (m).

Table 2 shows different upper integral limits x_u when $I = 1$ in eq. (36) for five slab depth locations. Table 3 illustrates the convergence of the inverse Hankel integral transform in predicting temperatures at these five different slab depths at 4:00 a.m. on June 28, 2003. Based on the convergence test, the minimum value for the upper integral limit (x_u) in Table 3 (Test No. 1) still gave 3 significant figure accuracy in the predicted temperature at all depths.

Table 1: Input parameters in model verification

Parameters	Value
<i>Thermal conductivity (Kcal/hr-m-°C)</i>	
PCC slab	1.85
Asphalt concrete base	1.38
Aggregate subbase	2.58
Subgrade	1.00
<i>Thermal diffusivity (m²/hr)</i>	
PCC slab	0.0035
Asphalt concrete base	0.0021
Aggregate subbase	0.0030
Subgrade	0.0030
Calibrated Absorptivity, a_s	0.50
Parameter to account for temperature variation along the radial direction (1/m), μ	0.002
Radial coordinate (m), r	0.00
Modified wind speed (m/s), v	3.5 to 5.0

Table 2: Values of upper integral limit, x_u when $I = 1$ for different depths z

z (m)	x_u (dimensionless)
0.0254	21
0.0762	9
0.1270	6
0.1778	3
0.2286	3

Table 3: Numerical convergence test results for the inverse Hankel integral transform (predicted temperatures at five different slab depths, °C)

Test No.	Slab Depth Z (m)				
	0.0254	0.0762	0.1270	0.1778	0.2286
1	20.6228784	23.0413174	24.9482524	26.3758674	27.3348095
2	20.6215549	23.0375610	24.9429443	26.3539092	27.3228534
3	20.6214680	23.0371050	24.9416775	26.3514324	27.3217703
4	20.6214579	23.0370260	24.9416126	26.3510673	27.3217703
5	20.6214557	23.0370067	24.9415936	26.3510028	27.3216457
6	20.6214553	23.0370047	24.9415857	26.3509899	27.3216288
7	20.6214552	23.0370042	24.9415851	26.3509871	27.3216263
8	20.6214551	23.0370040	24.9415848	26.3509865	27.3216263
9	20.6214551	23.0370040	24.9415847	26.3509863	27.3216259
10	20.6214551	23.0370040	24.9415847	26.3509863	27.3216258

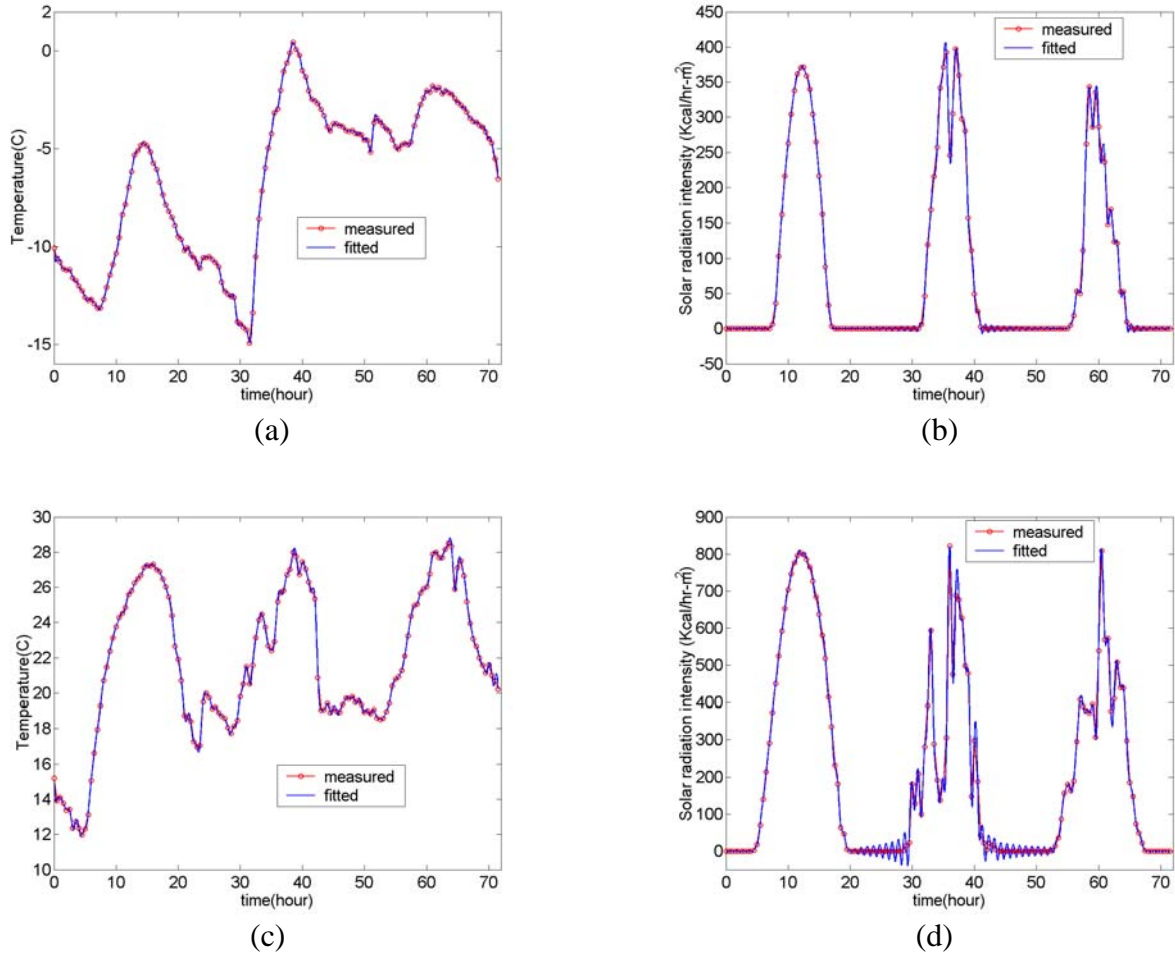
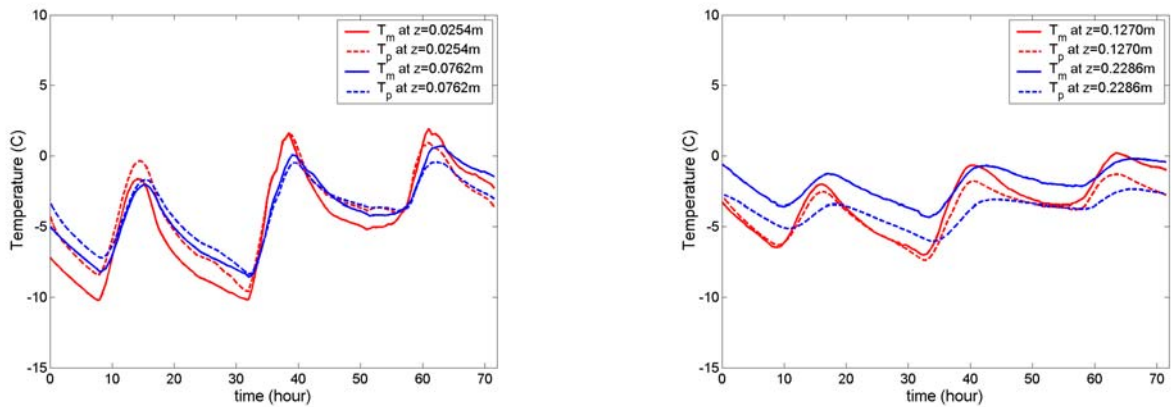


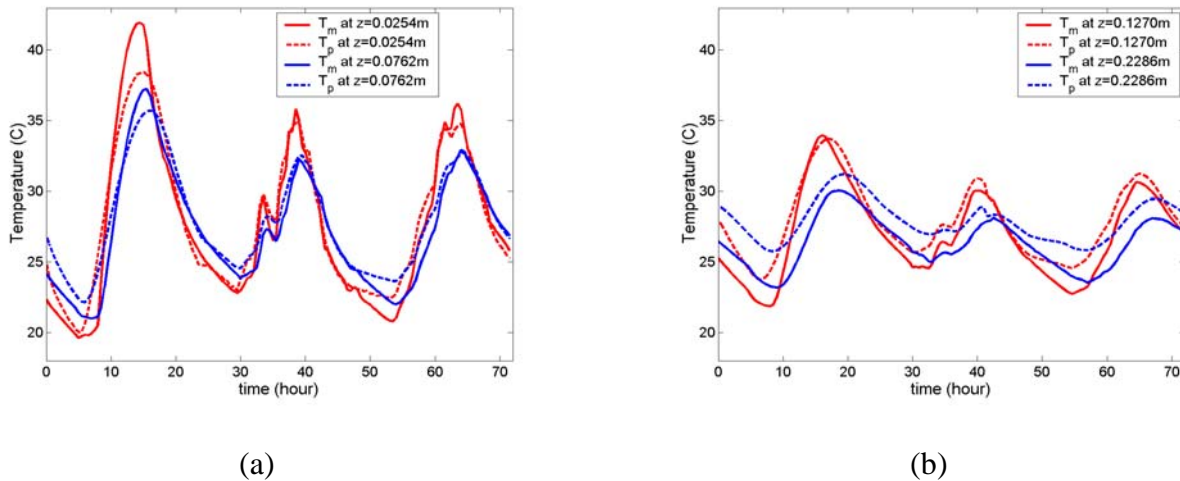
Figure 2. Measured and fitted air temperature (a,c) and solar radiation intensity (b,d) for three days in January and June 2003, respectively.

The predicted and measured pavement temperatures are plotted in Figures 3 and 4 for January and June 2003, respectively, at $z = 0.0254$ m, $z = 0.0762$ m, $z = 0.1270$ m, and $z = 0.2286$ m.



(a) (b)

Figure 3. Predicted (T_p) and measured (T_m) temperature for $z = 0.0254$ m, $z = 0.0762$ m (a) and $z = 0.1270$ m, $z = 0.2286$ m (b) in January 2003



(a) (b)

Figure 4. Predicted (T_p) and measured (T_m) temperature for $z = 0.0254$ m, $z = 0.0762$ m (a) and $z = 0.1270$ m, $z = 0.2286$ m (b) in June 2003

From Figures 3 and 4, it is clear that the largest temperature fluctuation with time occurs near the pavement surface ($z = 0.0254$ m) among the plotted four temperature depths. The farther from the pavement surface, the temperature variation with time is less. The highest pavement temperature of 42 °C occurred at $z = 0.0254$ m during the highest measured air temperature of 27.5 °C on June 28, 2003.

It is observed that the derived theoretical solution predicts reasonably good pavement temperature profile compared to the measured data. The maximum error between the predicted and measured temperature is around 3 °C for these two, three-day testing results except for one particular case, i.e. in predicting the temperature at $z = 0.0254$ m from the pavement surface at 8:00 a.m. on June 28, 2003, where the error between the predicted and measured temperature is around 5 °C.

Table 4 presents the mean errors and standard deviations between the predicted (T_p) and measured (T_m) temperature for each of five different slab depth locations. The mean error is the greatest near the bottom of the slab but the standard deviation is the largest near the top of the slab where temperature fluctuations are the greatest. The temperature discrepancy between the predicted and measured values come from many factors, such as the errors involved in selecting the appropriate material thermal parameters, e.g. thermal conductivity and thermal diffusivity; errors involved in the continuous interfacial heat flux assumptions, since different levels of heat flow resistance may exist in the interface of two consecutive pavement layers; deep soil

temperature effects; irradiation occurring at night and temperature measurement error. The irradiation at night and the effect of the deep soil temperature are likely the major reasons for the temperature discrepancy between the predicted and measured values. The irradiation in this paper is considered only by adjusting the absorptivity of the concrete and convection coefficient. Furthermore, the deep soil temperature cannot be currently considered with the proposed analytical approach.

Table 4: Mean errors between predicted and measured temperature at different depths ($^{\circ}\text{C}$), i.e. $T_p - T_m$ (values in bracket denote standard deviations of temperature error)

Date	Slab Depth Location z (m)				
	0.0254	0.0762	0.1270	0.1778	0.2286
Jan.12 to Jan. 14, 2003	0.80 (0.97)	0.12 (0.74)	-0.53 (0.57)	-1.19 (0.43)	-1.91 (0.34)
June 28 to June 30, 2003	0.31 (1.36)	0.68 (0.92)	1.06 (0.74)	1.37 (0.64)	1.63 (0.60)

Comments on the Proposed Analytical Solution

The proposed analytical solution can rapidly, yet reasonably, predict the temperature field in the N-layered pavement system with limited input data, which is especially important for characterizing field temperature profile when using the falling weight deflectometer (FWD) test device. In particular, the initial pavement temperature profile is not required in order to implement this solution. A simplification of the proposed model to accommodate limited weather data could be made to just use the maximum and minimum air temperatures for the day along with the peak solar radiation intensity for the day. Furthermore, for FWD testing conducted during the daytime hours, only the surface layer's temperature profile are required thus allowing for usage of a more realistic surface absorptivity value.

The proposed analytical solution can also serve as a driving engine to generate the initial pavement temperature profile for other numerical treatments of temperature field, such as in simulating temperature evolution of "hydrating" concrete pavement where the heat of hydration plays an important role and its value is related to the initial pavement temperature profile. Also, this 2-D model result can be easily implemented for 1-D case by simply setting $r = 0$ and Bessel function $J_0(0) = 1$ in eq. (35).

CONCLUSIONS

The theoretical solution of 2-D axisymmetric temperature field in a multi-layered pavement system is successfully derived. The temperature at any pavement location (r, z) and time t in an N-layered pavement system can be calculated by using this solution under the cylindrical coordinate system. Hankel integral transformation with respect to the radial coordinate is utilized in the derivation of solution. The interpolatory trigonometric polynomials that are based on discrete Fourier transform are used to fit the measured air temperatures and solar radiation intensities during a day, which are essential components in the boundary condition for the

underlying heat transfer problem. Field temperature testing results demonstrate that the derived analytical solution generates realistic temperature profiles in a concrete slab for a 4-layered rigid pavement system. The advantage of this formulation is that it can rapidly predict the pavement temperature field for short time durations with limited input data and it does not require the initial temperature field to be known.

ACKNOWLEDGEMENT

Financial support for this study was based on the results of ICT-R57, Evaluation And Implementation of Improved CRCP and JPCP Design Methods For Illinois. ICT-R57 was conducted in cooperation with the Illinois Center for Transportation; the Illinois Department of Transportation, Division of Highways; and the U.S. Department of Transportation, Federal Highway Administration.

APPENDIX

This appendix summarizes the main variables and symbols used in the derivation and formulation of analytical solution of temperature field in N-layered pavement system (25).

In the following, the subscript i runs from 1 to n except stated explicitly otherwise, the superscript k, l runs from 1 to 2 with understanding that they are not taken as powers; symbol like CA in $(CA)_i$ is treated as a single variable.

n = total layers of pavement system including subgrade

r = radial coordinate in the cylindrical coordinate system (m)

z = vertical coordinate in the cylindrical coordinate system (m)

$T_i(r, z, t)$ = function of i th layer temperature field ($^{\circ}\text{C}$)

h_i = thickness of i th pavement layer (m), $i = 1, 2, \dots, n-1$

λ_i = thermal conductivity of i th pavement layer (Kcal/m-hr- $^{\circ}\text{C}$)

α_i = thermal diffusivity of i th pavement layer (m^2/hr)

$$H_i = \sum_{j=1}^i h_j, \quad i = 1, 2, \dots, n-1 \quad (\text{A-1})$$

q = heat flux into pavement (Kcal/ m^2 -hr)

P = heat flux caused by the convection due to temperature difference between atmosphere and pavement surface (Kcal/ m^2 -hr)

R = net solar radiation flux (Kcal/ m^2 -hr)

$T_a(t)$ = air temperature ($^{\circ}\text{C}$)

A = magnitude of wave mode used in the model boundary condition ($^{\circ}\text{C}$)

B = pavement surface convection coefficient (Kcal/ m^2 -hr- $^{\circ}\text{C}$)

C_i, D_i = integration constants for layer i

a_s = surface absorptivity to the total solar radiation (dimensionless)

$Q(t)$ = solar radiation flux (Kcal/m² · hr)

$F(t)$ = irradiation flux emitted by pavement surface (Kcal/m² · hr)

μ = parameter used in the radial temperature variation function $f(r)$

$Y_i(r, z, t)$ = function of i th layer temperature field in the complex plane (°C)

ω = frequency of wave mode used in the model boundary condition (1/hr)

ξ = transformation variable used in the Hankel integral transform

j = imaginary unit number with $j^2 = -1$

$$v_i = \sqrt{1 + \frac{\omega^2}{\alpha_i^2 \xi^4}} \quad (\text{A-2})$$

$$M_i = \sqrt{\frac{v_i + 1}{2}} \quad (\text{A-3})$$

$$N_i = \sqrt{\frac{v_i - 1}{2}} \quad (\text{A-4})$$

$$\gamma_i = \arctan\left(\sqrt{\frac{v_i - 1}{v_i + 1}}\right) \quad (\text{A-5})$$

$$(CA)_i = \xi H_i(N_{i+1} - N_i), \quad i = 1, 2, \dots, n-1 \quad (\text{A-6a})$$

$$(CB)_i = \xi H_i(N_{i+1} + N_i), \quad i = 1, 2, \dots, n-1 \quad (\text{A-6b})$$

$$(CC)_i = \gamma_i - \gamma_{i+1}, \quad i = 1, 2, \dots, n-1 \quad (\text{A-6c})$$

$$(CD)_i = \frac{\lambda_i}{\lambda_{i+1}} \sqrt{\frac{v_i}{v_{i+1}}}, \quad i = 1, 2, \dots, n-1 \quad (\text{A-6d})$$

$$(CH)_i = -2\xi H_i M_i + \xi H_{i-1}(M_i + M_{i-1}) \quad (\text{A-6e})$$

$$(CK)_i = -\xi H_{i-1}(M_i - M_{i-1}) \quad (\text{A-6f})$$

$$P_i^{11} = \frac{1}{2} [e^{j\xi \cdot H_i(N_{i+1} - N_i)} + (CD)_i \cdot e^{j(\xi \cdot H_i(N_{i+1} - N_i) + \gamma_i - \gamma_{i+1})}] \quad (\text{A-7a})$$

$$P_i^{12} = \frac{1}{2} [e^{j\xi \cdot H_i(N_{i+1} + N_i)} - (CD)_i \cdot e^{j(\xi \cdot H_i(N_{i+1} + N_i) + \gamma_i - \gamma_{i+1})}] \quad (\text{A-7b})$$

$$P_i^{21} = \frac{1}{2} [e^{-j\xi \cdot H_i(N_{i+1} + N_i)} - (CD)_i \cdot e^{j(-\xi \cdot H_i(N_{i+1} + N_i) + \gamma_i - \gamma_{i+1})}] \quad (\text{A-7c})$$

$$P_i^{22} = \frac{1}{2} [e^{j\xi \cdot H_i(N_i - N_{i+1})} + (CD)_i \cdot e^{j(\xi \cdot H_i(N_i - N_{i+1}) + \gamma_i - \gamma_{i+1})}] \quad (\text{A-7d})$$

where $i = 1, 2, \dots, n-1$ in eq. (A-7a) to (A-7d).

$$P_i^{kl} = F_i^{kl} e^{j\beta_i^{kl}}, \quad i = 1, 2, \dots, n-1 \quad (\text{A-8})$$

$$R_i^{kl} = K_i^{kl} e^{j\psi_i^{kl}} \quad (\text{A-9})$$

$$R_1^{kl} = P_1^{kl} \quad (\text{A-10})$$

$$R_i^{11} = e^{-2\xi H_i M_i + \xi H_{i-1}(M_i + M_{i-1})} P_i^{11} R_{i-1}^{11} + e^{-\xi H_{i-1}(M_i - M_{i-1})} P_i^{12} R_{i-1}^{21} \quad (\text{A-11a})$$

$$R_i^{12} = e^{-2\xi H_i M_i + \xi H_{i-1}(M_i + M_{i-1})} P_i^{11} R_{i-1}^{12} + e^{-\xi H_{i-1}(M_i - M_{i-1})} P_i^{12} R_{i-1}^{22} \quad (\text{A-11b})$$

$$R_i^{21} = e^{-2\xi H_i M_i + \xi H_{i-1}(M_i + M_{i-1})} P_i^{21} R_{i-1}^{11} + e^{-\xi H_{i-1}(M_i - M_{i-1})} P_i^{22} R_{i-1}^{21} \quad (\text{A-11c})$$

$$R_i^{22} = e^{-2\xi H_i M_i + \xi H_{i-1}(M_i + M_{i-1})} P_i^{21} R_{i-1}^{12} + e^{-\xi H_{i-1}(M_i - M_{i-1})} P_i^{22} R_{i-1}^{22} \quad (\text{A-11d})$$

where $i = 2, 3, \dots, n$ in eq. (A-11a)-(A-11d).

$$F_i^{11} = \frac{1}{2} \sqrt{[\cos(CA)_i + (CD)_i \cos((CA)_i + (CC)_i)]^2 + [\sin(CA)_i + (CD)_i \sin((CA)_i + (CC)_i)]^2} \quad (\text{A-12a})$$

$$F_i^{12} = \frac{1}{2} \sqrt{[\cos(CB)_i - (CD)_i \cos((CB)_i + (CC)_i)]^2 + [\sin(CB)_i - (CD)_i \sin((CB)_i + (CC)_i)]^2} \quad (\text{A-12b})$$

$$F_i^{21} = \frac{1}{2} \sqrt{[\cos(-(CB)_i) - (CD)_i \cos(-(CB)_i + (CC)_i)]^2 + [\sin(-(CB)_i) - (CD)_i \sin(-(CB)_i + (CC)_i)]^2} \quad (\text{A-12c})$$

$$F_i^{22} = \frac{1}{2} \sqrt{[\cos(-(CA)_i) + (CD)_i \cos(-(CA)_i + (CC)_i)]^2 + [\sin(-(CA)_i) + (CD)_i \sin(-(CA)_i + (CC)_i)]^2} \quad (\text{A-12d})$$

where $i = 1, 2, \dots, n-1$ in eq. (A-12a)-(A-12d).

Argument β_i^{11} associated with F_i^{11} ($i = 1, 2, \dots, n-1$) can be determined as follows:

Let $\Phi = \cos(CA)_i + (CD)_i \cos((CA)_i + (CC)_i)$, $\Psi = \sin(CA)_i + (CD)_i \sin((CA)_i + (CC)_i)$

$$(1) \text{ If } \Phi > 0 \ \& \ \Psi \geq 0 \text{ or } \Phi > 0 \ \& \ \Psi \leq 0, \text{ then } \beta_i^{11} = \arctan \frac{\Psi}{\Phi} \quad (\text{A-13a})$$

$$(2) \text{ If } \Phi < 0 \ \& \ \Psi \geq 0 \text{ or } \Phi < 0 \ \& \ \Psi \leq 0, \text{ then } \beta_i^{11} = \arctan \frac{\Psi}{\Phi} + \pi \quad (\text{A-13b})$$

$$(3) \text{ If } \Phi = 0 \ \& \ \Psi > 0, \text{ then } \beta_i^{11} = \frac{\pi}{2} \quad (\text{A-13c})$$

$$(4) \text{ If } \Phi = 0 \ \& \ \Psi < 0, \text{ then } \beta_i^{11} = \frac{3\pi}{2} \quad (\text{A-13d})$$

$$(5) \text{ If } \Phi = 0 \ \& \ \Psi = 0, \text{ then } \beta_i^{11} = 0 \quad (\text{A-13e})$$

$\beta_i^{12}, \beta_i^{21}, \beta_i^{22}$ can be obtained analogously.

$$K_1^{kl} = F_1^{kl} \quad (\text{A-14a})$$

$$\psi_1^{kl} = \beta_1^{kl} \quad (\text{A-14b})$$

$$K_i^{11} = \{ [e^{(CH)_i} F_i^{11} K_{i-1}^{11} \cos(\beta_i^{11} + \psi_{i-1}^{11}) + e^{(CK)_i} F_i^{12} K_{i-1}^{21} \cos(\beta_i^{12} + \psi_{i-1}^{21})]^2 + [e^{(CH)_i} F_i^{11} K_{i-1}^{11} \sin(\beta_i^{11} + \psi_{i-1}^{11}) + e^{(CK)_i} F_i^{12} K_{i-1}^{21} \sin(\beta_i^{12} + \psi_{i-1}^{21})]^2 \}^{\frac{1}{2}} \quad (\text{A-15a})$$

$$K_i^{12} = \{ [e^{(CH)_i} F_i^{11} K_{i-1}^{12} \cos(\beta_i^{11} + \psi_{i-1}^{12}) + e^{(CK)_i} F_i^{12} K_{i-1}^{22} \cos(\beta_i^{12} + \psi_{i-1}^{22})]^2 + [e^{(CH)_i} F_i^{11} K_{i-1}^{12} \sin(\beta_i^{11} + \psi_{i-1}^{12}) + e^{(CK)_i} F_i^{12} K_{i-1}^{22} \sin(\beta_i^{12} + \psi_{i-1}^{22})]^2 \}^{\frac{1}{2}} \quad (\text{A-15b})$$

$$K_i^{21} = \{ [e^{(CH)_i} F_i^{21} K_{i-1}^{11} \cos(\beta_i^{21} + \psi_{i-1}^{11}) + e^{(CK)_i} F_i^{22} K_{i-1}^{21} \cos(\beta_i^{22} + \psi_{i-1}^{21})]^2 + [e^{(CH)_i} F_i^{21} K_{i-1}^{11} \sin(\beta_i^{21} + \psi_{i-1}^{11}) + e^{(CK)_i} F_i^{22} K_{i-1}^{21} \sin(\beta_i^{22} + \psi_{i-1}^{21})]^2 \}^{\frac{1}{2}} \quad (\text{A-15c})$$

$$K_i^{22} = \{ [e^{(CH)_i} F_i^{21} K_{i-1}^{12} \cos(\beta_i^{21} + \psi_{i-1}^{12}) + e^{(CK)_i} F_i^{22} K_{i-1}^{22} \cos(\beta_i^{22} + \psi_{i-1}^{22})]^2 + [e^{(CH)_i} F_i^{21} K_{i-1}^{12} \sin(\beta_i^{21} + \psi_{i-1}^{12}) + e^{(CK)_i} F_i^{22} K_{i-1}^{22} \sin(\beta_i^{22} + \psi_{i-1}^{22})]^2 \}^{\frac{1}{2}} \quad (\text{A-15d})$$

where $i = 2, 3 \dots n-1$ in eq. (A-15a)-(A-15d).

Argument ψ_i^{kl} associated with K_i^{kl} ($i = 2, \dots, n$) can be obtained analogously in determining β_i^{11} above.

$$G_1 = -\xi \sqrt{v_1} e^{-2\xi H_1 M_1} \frac{K_{n-1}^{21}}{K_{n-1}^{22}} \cos(\psi_{n-1}^{21} - \psi_{n-1}^{22} + \gamma_1) - \xi \sqrt{v_1} \cos \gamma_1 + \frac{B}{\lambda_1} \cdot \frac{K_{n-1}^{21}}{K_{n-1}^{22}} e^{-2\xi H_1 M_1} \cos(\psi_{n-1}^{21} - \psi_{n-1}^{22}) - \frac{B}{\lambda_1} \quad (\text{A-16a})$$

$$G_2 = -\xi \sqrt{v_1} e^{-2\xi H_1 M_1} \frac{K_{n-1}^{21}}{K_{n-1}^{22}} \sin(\psi_{n-1}^{21} - \psi_{n-1}^{22} + \gamma_1) - \xi \sqrt{v_1} \sin \gamma_1 + \frac{B}{\lambda_1} \cdot \frac{K_{n-1}^{21}}{K_{n-1}^{22}} e^{-2\xi H_1 M_1} \sin(\psi_{n-1}^{21} - \psi_{n-1}^{22}) \quad (\text{A-16b})$$

Argument τ_1 associated with G_1 and G_2 can be obtained analogously in determining β_i^{11} above by setting $G_1 = \Phi$ and $G_2 = \Psi$.

$$\Gamma_1 = -\frac{\mu A \cdot B}{\lambda_1} \frac{\sqrt{(\mu^2 + \xi^2)(G_1^2 + G_2^2)}}{(\mu^2 + \xi^2)(G_1^2 + G_2^2)} \quad (\text{A-17a})$$

$$\Gamma_2 = -\Gamma_1 \frac{K_{n-1}^{21}}{K_{n-1}^{22}} e^{-2\xi H_1 M_1} \quad (\text{A-17b})$$

$$(SC)_i = e^{-2\xi H_1 M_1} K_{i-1}^{11} \cdot \Gamma_1 \quad (\text{A-18a})$$

$$(SD)_i = K_{i-1}^{12} \cdot \Gamma_2 \quad (\text{A-18b})$$

$$(SE)_i = \psi_{i-1}^{12} + \psi_{n-1}^{21} - \psi_{n-1}^{22} - \tau_1 \quad (\text{A-18c})$$

$$(SF)_i = \psi_{i-1}^{11} - \tau_1 \quad (\text{A-18d})$$

$$(SG)_i = e^{-2\xi H_1 M_1} K_{i-1}^{21} \cdot \Gamma_1 \quad (\text{A-18e})$$

$$(SH)_i = K_{i-1}^{22} \cdot \Gamma_2 \quad (\text{A-18f})$$

$$(SK)_i = \psi_{i-1}^{22} + \psi_{n-1}^{21} - \psi_{n-1}^{22} - \tau_1 \quad (\text{A-18g})$$

$$(SJ)_i = \psi_{i-1}^{21} - \tau_1 \quad (\text{A-18h})$$

where $i = 2, 3 \dots n$ in eq. (A-18a)-(A-18h).

$$\Delta_{11} = \Gamma_1 \quad (\text{A-19a})$$

$$\delta_{11} = -\tau_1 \quad (\text{A-19b})$$

$$\Delta_{12} = \Gamma_2 \quad (\text{A-19c})$$

$$\delta_{12} = \psi_{n-1}^{21} - \psi_{n-1}^{22} - \tau_1 \quad (\text{A-19d})$$

$$\Delta_{i1} = \sqrt{[(SC)_i \cos(SF)_i + (SD)_i \cos(SE)_i]^2 + [(SC)_i \sin(SF)_i + (SD)_i \sin(SE)_i]^2} \quad (\text{A-20a})$$

$$\Delta_{i2} = \sqrt{[(SG)_i \cos(SJ)_i + (SH)_i \cos(SK)_i]^2 + [(SG)_i \sin(SJ)_i + (SH)_i \sin(SK)_i]^2} \quad (\text{A-20b})$$

$$\Delta_{n2} = 0 \quad (\text{A-20c})$$

where $i = 2, 3 \dots n$ in eq. (A-20a) and $i = 2, 3 \dots n-1$ in eq. (A-20b).

$$C_1 = \Gamma_1 e^{-j\tau_1} \quad (\text{A-21a})$$

$$D_1 = \Gamma_2 e^{j(\psi_{n-1}^{21} - \psi_{n-1}^{22} - \tau_1)} \quad (\text{A-21b})$$

$$C_i = \Delta_{i1} e^{j\delta_{i1}} \cdot e^{\xi H_{i-1}(M_i + M_{i-1})}, \quad i = 2, 3 \dots n \quad (\text{A-21c})$$

$$D_i = \Delta_{i2} e^{j\delta_{i2}} \cdot e^{-\xi H_{i-1}(M_i - M_{i-1})}, \quad i = 2, 3 \dots n-1 \quad (\text{A-21d})$$

$$D_n = 0 \quad (\text{A-21e})$$

where $i = 2, 3 \dots n$ in eq. (A-21c) and $i = 2, 3 \dots n-1$ in eq. (A-21d), and arguments δ_{i1}, δ_{i2} can be obtained analogously in determining β_i^{11} , for example, to determine δ_{i1} , replacing Φ, Ψ in (A-13) by

$$\Phi = (SC)_i \cos((SF)_i) + (SD)_i \cos((SE)_i)$$

$$\Psi = (SC)_i \sin((SF)_i) + (SD)_i \sin((SE)_i)$$

REFERENCES

1. Huang, Y. H. *Pavement Analysis and Design*, 2nd edition, Pearson Education, Inc., 2004.
2. Tschoegl, N. W. *The phenomenological Theory of Linear Viscoelastic Behavior: An Introduction*, Springer-Verlag, 1989.
3. Westergaard, H. M. Analysis of Stresses in Concrete Pavement Due to Variations of Temperature. *Proceedings, Highway Research Board*, Vol. 6, 1926, pp. 201-215.
4. Darter, M. I., and E. J. Barenberg. *Design of Zero-Maintenance Plain Jointed Concrete Pavement*. Publication FHWA-RD-77-111, Vol.1. FHWA, U.S. Department of Transportation, 1977.
5. ARA, Inc. *Guide for Mechanistic-Empirical Design of New and Rehabilitated Pavement Structures. Final Report*. National Cooperative Highway Research Program Project 1-37A, 2004.
6. Barber, E. S. Calculation of Maximum Pavement Temperatures from Weather Reports. *Highway Research Board Bulletin 168*, National Research Council, Washington, D.C., 1957, pp. 1-8.
7. Rumney, T. N., and R. A. Jimenez. Pavement Temperatures in the Southwest. *Highway Research Record No. 361*, National Research Council, Washington, D.C., 1969, pp. 1-13.
8. Lukanen, E. O., C. Han, and E. L. Jr. Skok. Probabilistic Method of Asphalt Binder Selection Based on Pavement Temperature. In *Transportation Research Record 1609*, TRB, National Research Council, Washington, D.C., 1998, pp. 12-20.

9. Diefenderfer, B. K., I. L. Al-Qadi, and S. D. Diefenderfer. Model to Predict Pavement Temperature Profile: Development and Validation. *ASCE Journal of Transportation Engineering*, Vol. 132, No. 2, 2006, pp. 162-167.
10. Dempsey, B. J., and M. R. Thompson. A Heat Transfer Model for Evaluating Frost Action and Temperature Related Effects in Multilayered Pavement Systems. *Highway Research Record No. 342*, National Research Council, Washington, D.C., 1970, pp. 39-56.
11. Hsieh, C. K., C. Qin, and E. E. Ryder. Development of Computer Modeling for Prediction of Temperature Distribution Inside Concrete Pavements. *Report Number FL/DOT/SMO/90-374, Final Report to Florida Department of Transportation, 1989.*
12. Rasmussen, R. O., J. M. Ruiz, D. K. Rozycki, and B. F. McCullough. Constructing High-Performance Concrete Pavements with FHWA HIPERPAV Systems Analysis Software. In *Transportation Research Record 1813*, Transportation Research Board, Washington, D.C., 2002, pp. 11-20.
13. Schindler, A. K., J. M. Ruiz, R. O. Rasmussen, G. K. Chang, and L. G. Wathne. Concrete Pavement Temperature Prediction and Case Studies with the FHWA HIPERPAV models. *Cement and Concrete Composites 26 (2004)*, pp. 463-471.
14. Yavuzturk, C., K. Ksaibati, and A. D. Chiasson. Assessment of Temperature Fluctuations in Asphalt Pavements Due to Thermal Environmental Conditions Using a Two-Dimensional, Transient Finite-Difference Approach. *Journal of Materials in Civil Engineering*, Vol. 17, No. 4, 2005, pp. 465-475.
15. Solaimanian, M., and T. W. Kennedy. Predicting Maximum Pavement Surface Temperature Using maximum Air Temperature and Hourly Solar Radiation. In *Transportation Research Record 1417*, Transportation Research Board, Washington, D.C., 1993, pp. 1-11.
16. Liang, R. Y., and Y-Z. Niu. Temperature and Curling Stress in Concrete Pavements: Analytical Solution. *ASCE Journal of Transportation Engineering*, Vol. 124, No. 1, 1998, pp. 91-100.
17. Burmister, D. M. The General Theory of Stresses and Displacements in Layered Soil Systems. *Journal of Applied Physics*, Vol. 16, 1945, pp. 84-94, 126-127, 296-302.
18. Straub, A. L., H. N. Jr. Schenck, and F. E. Przybycien. (1968). Bituminous Pavement Temperature Related to climate. *Highway Research Record 256*, 1968, pp. 53-77.
19. Wu, Ganchang. The Analytic Theory of the Temperature Fields of Bituminous Pavement Over Semi-rigid Roadbase. *Applied Mathematics and Mechanics (English version)*, Vol. 18, No.2, Feb. 1997.
20. Branco, F.A., R. A. Mendes, and E. H. Mirabell. Heat of Hydration Effects in Concrete Structures. *ACI Mater. J.*, 89(2), 1992, pp. 139-145.
21. Burden, R. L., and J. D. Faires. *Numerical Analysis*. 7th edition, Brooks/Cole, 2001.
22. Powers, David L. *Boundary Value Problems*, 4th edition, Harcourt Academic Press, 1999.
23. Sneddon, I. N. *The Use of Integral Transforms*, McGraw-Hill Book Company, 1972.
24. Kohler, E., G. Long, and J. Roesler. Construction of Extended Life Continuously Reinforced Concrete Pavement at ATREL. *Transportation Engineering Series No. 126, Illinois Cooperative Highway and Transportation Series No. 282, UILU-ENG-2002-2009*, University of Illinois, Urbana, IL, 2002, 54 pp.
25. Wang, D. *Analytical Solution of Temperature Field and Thermal Stress in Multi-layered Asphalt Pavement Systems*. M. Sc. Thesis, School of Transportation Science and Engineering, Harbin Institute of Technology, 1996 (in Chinese).